Simulation Conditions to Compute the Dispersion Diagram of 3D Periodic Structures

HAIRU WANG [1] **(Graduate Student Member, IEEE),**
OSKAR ZETTERSTROM [1] **(Graduate Student Member, IEEE),**
PILAR CASTILLO-TAPIA [1] **(Graduate Student Member, IEEE), FRANCISCO MESA** [2] **(Fellow, IEEE),**
AND OSCAR QUEVEDO-TERUEL [1] **(Fellow, IEEE)**

(Regular Paper)

[1]Division of Electromagnetic Engineering and Fusion Science, KTH Royal Institute of Technology, SE-100 44 Stockholm, Sweden
[2]Department of Applied Physics 1, Universidad de Sevilla, 41004 Sevilla, Spain

CORRESPONDING AUTHOR: Oscar Quevedo-Teruel (e-mail: oscarqt@kth.se).

ABSTRACT In this work, we examine the methodology for numerically computing the dispersion diagram of three-dimensional periodic structures using commercial electromagnetic simulators. Examples of periodic structures based on body-centered cubic, face-centered cubic, and monoclinic lattices are used to illustrate this methodology. We first outline the characteristics of these structures in both physical and reciprocal spaces from a theoretical point of view. On this basis, we provide a comprehensive explanation of how to adjust the setting in simulation software commonly used in microwave engineering to generate the dispersion diagrams of these structures. The appropriate simulation conditions are tabulated to serve as a further guide for other researchers. This study also explores the influence of the elements of the unit cell on the dispersion characteristics. Additionally, we evaluate and contrast the dispersion properties of identical periodic elements when having simple cubic, body-centered cubic, and face-centered cubic arrangements. We found that symmetries, such as those seen in body-centered cubic and face-centered cubic arrangements, can improve the isotropy and maintain low-dispersion characteristics over a wider frequency range. The monoclinic structure is also taken as an example to demonstrate that the reported analysis method can be applied to the dispersion analysis of other more complex noncubic lattices. Our findings offer useful information for the examination and engineering of three-dimensional periodic structures, which can be used to design microwave and antenna devices.

INDEX TERMS 3D periodic structure, body-centered cubic lattice, dispersion analysis, electromagnetic simulation, face-centered cubic lattice, monoclinic lattice.

I. INTRODUCTION

Periodic structures consist of elementary units (atoms, molecules, metallo-dielectric elements, etc.) that are repeated regularly at fixed spatial intervals, giving rise to structural ordering. Manipulation of the geometric and material parameters of these unit cells can alter the properties of electromagnetic waves as they propagate through the periodic arrangement, providing significant flexibility in device design [1], [2], [3], [4], [5], [6], [7]. In the field of microwave engineering, these structures are widely used in the design of multiple devices, such as filters, frequency-selective surfaces, leaky wave antennas and lenses [8], [9], [10], [11], [12], [13]. The most common method to analyze and characterize the properties of periodic structures is to study their dispersion diagram [14], [15]. This dispersion diagram represents the relationship between frequency and wavevector, providing valuable information on phase/group velocity, attenuation, stopband, and coupling between modes [16], [17]. This information is crucial in determining the geometric/material parameters of the unit cell in the design of propagating/filtering/radiating devices.

In most cases, engineered periodic structures are arranged in a rectangular two-dimensional (2D) configuration

[18], [19] or a simple cubic (sc) three-dimensional (3D) configuration [20], [21]. For 3D periodic structures, studies have explored configurations with symmetries. The study revealed that the body-centered cubic (bcc) and face-centered cubic (fcc) structures are more isotropic and less dispersive over a larger frequency range compared to the sc configuration [22], [23], [24]. However, these studies did not introduce a method for the dispersion analysis of 3D periodic structures, especially those based on more complex configurations.

Several methods exist for computing dispersion diagrams of periodic structures. For example, equivalent circuit analysis methods [25], multimodal transfer matrix method [26], [27], [28], Floquet analysis of the structure [29], etc. These methods are efficient in analyzing 2D periodic structures with rectangular configurations or 3D periodic structures with simple cubic configurations. However, when confronted with 3D periodic elements featuring complex geometries such as truncated octahedra shape or dodecahedra shape, computational complexity escalates significantly. Furthermore, these methods often require the use of in-house code to calculate dispersion diagrams, which may pose initial challenges in terms of usability and application. Compared to the computational methods mentioned above, commercial software with appropriate settings can directly simulate and obtain the dispersion diagrams of various periodic structures, even those with complex geometric and/or material configurations. While it is not possible to directly extract material losses from the eigensolver tool of commercial software packages, the ability to calculate dispersion diagrams related to phase shifts (which only involves the obtaining of the phase constant β) is typically adequate to meet needs, thus not hindering the common practice of using commercial software to study dispersion diagrams of periodic structures.

In this paper, we use the bcc and fcc structures as examples to explain in detail how to utilize commercial software (ANSYS HFSS is employed in this study) to obtain the dispersion diagram of a 3D periodic structure. In particular, we discuss and describe the conditions that must be set in the eigensolver tool of the simulation package. This enables us to conduct a further detailed analysis and comparison of the electromagnetic wave dispersion properties of the sc, bcc, and fcc structures when the physical periodic elements are metallic spheres and metallic cuboids. The analysis technique discussed in this study can be easily utilized for other 3D periodic structures that possess noncubic lattices. The paper employs a monoclinic lattice as an illustration of this concept. Our primary objective is to offer a basis for the future development of microwave and antenna devices that rely on 3D periodic structures.

The structure of this paper is as follows. Section II describes a general method for the analysis of the dispersion of 3D periodic structures, revisiting some important concepts. In Section II-A, an analysis of periodic structures in physical space is presented, while Section II-B studies periodic structures in reciprocal space (the space associated with wavevectors). Section III-A presents the modeling and

analysis of periodic structures composed of metallic spheres. In Section III-B, the modeling and analysis are extended to periodic structures composed of metallic cuboids. The monoclinic structure is used as an example in Section IV-A on how to perform a dispersion analysis on more complex, noncubic 3D periodic structures. Section IV-B presents the modeling and the simulation results of this monoclinic structure. Some relevant final conclusions are summarized in Section V.

II. DISPERSION ANALYSIS OF THREE-DIMENSIONAL PERIODIC STRUCTURES

This section gives a brief outline of how to model and find the dispersion diagrams of 3D periodic structures. The bcc structure is chosen as an example from a theoretical point of view. Additionally, the conditions for configuring the structure in popular simulation software packages are outlined. This analysis and simulation setting can be easily adapted to other 3D periodic structures.

A. PHYSICAL SPACE

The fundamental building block of a periodic structure, referred to as the "unit cell" [14], [16], is periodically arranged and repeated in space to construct the periodic structure. Inspired by the study of solid state physics, the concept of a "lattice" is used to synthesize the geometric layout of periodic structures [14], [16]. Each point on the lattice is associated with a unit cell, and the lattice does not depend on the particular element that comprises the unit cell. This lattice is known as the "Bravais lattice" if the arrangement and orientation of the lattice points remain invariant at any point within the lattice. Each Bravais lattice is characterized by a fundamental set of translation vectors, typically described as $(\mathbf{a}_1, \mathbf{a}_2, \mathbf{a}_3)$ in a 3D space, and these vectors relate the position of the lattice points within the structure following $n_1\mathbf{a}_1 + n_2\mathbf{a}_2 + n_3\mathbf{a}_3, n_i \in \mathbf{Z}$. These translation vectors are also called "lattice vectors" and are instrumental in defining the periodic arrangement of lattice points in the Bravais lattice.

When the Bravais lattice is defined in real or physical space, it is also called a 'direct lattice' or 'physical lattice'. Fig. 1 illustrates the corresponding physical lattice for unit cells organized in a bcc configuration. In the upper left of the lattice arrangement, nine lattice points are highlighted in purple. These highlighted points show how the lattice point at the center of a body-centered cube connects to other lattice points. In this case, the associated lattice vectors are expressed as

$$\mathbf{a}_1 = a\left(\frac{1}{2}\hat{\mathbf{x}} - \frac{1}{2}\hat{\mathbf{y}} - \frac{1}{2}\hat{\mathbf{z}}\right)$$

$$\mathbf{a}_2 = a\left(\frac{1}{2}\hat{\mathbf{x}} + \frac{1}{2}\hat{\mathbf{y}} - \frac{1}{2}\hat{\mathbf{z}}\right)$$

$$\mathbf{a}_3 = a\left(\frac{1}{2}\hat{\mathbf{x}} - \frac{1}{2}\hat{\mathbf{y}} + \frac{1}{2}\hat{\mathbf{z}}\right) \quad (1)$$

where a is the distance between a lattice point and its second closest lattice point (also indicated in the figure).
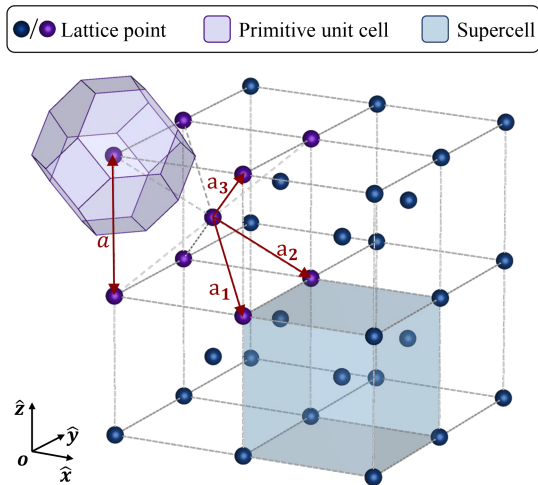
FIGURE 1. Physical lattice when 3D periodic structures are organized in a bcc configuration.

Usually, periodic structure analysis is carried out in a minimal region around a Bravais lattice point, called "the primitive unit cell". This region occupies the minimum volume that can fill the full space without overlapping or leaving gaps when copied and translated along the lattice vectors. An example of a possible primitive unit cell for a bcc configuration is shown as a purple-shaded polyhedron in Fig. 1. There can be multiple choices for this primitive unit cell, each with the same volume and containing exactly one lattice point. However, we note that for some choices, the primitive unit cell may not fully display the symmetry of the Bravais lattice, and the concept of a Wigner-Seitz (WS) cell is introduced to clearly exhibit the symmetry of the lattice [14]. The primitive unit cell shown in Fig. 1 is, in fact, the WS cell of the bcc structure. In contrast to the primitive unit cell, a cell that can also fill the entire space but has a relatively larger volume is called a supercell (this supercell will always enclose more than one lattice point). The blue-shaded region in Fig. 1 shows a possible cubic supercell associated with the bcc structure, and we observe that this cubic cell contains two lattice points (one at the center of the cell and one formed by the contribution of 1/8th of a point from each corner).

Given that the WS cell represents the minimum volume that encompasses the full symmetry of periodic structures, it is often the preferred choice for studying their properties, particularly when the WS cell exhibits a relatively simple configuration. However, in some periodic structures, the shape of a WS cell can be complicated, which poses challenges for its direct analysis. In such cases, researchers may turn to studying a corresponding supercell of the periodic structure with a simpler shape. For instance, when looking into the dispersion characteristics of periodic structures, eigenmode solvers of commercial software programs are commonly used to generate dispersion diagrams. These programs can be more difficult to use when the unit cell has nonorthogonal faces or sides. As a result, we may opt to simulate the supercell of the periodic structure instead of the more intricate primitive unit cell.

B. RECIPROCAL SPACE

The mathematical dual lattice of the physical lattice is called the reciprocal lattice, which is the Bravais lattice in the reciprocal space [14]. The reciprocal lattice contains information about the wavevectors of those plane waves with the same periodicity as the respective physical Bravais lattice and also reflects the periodicity of these wavevectors [14], [16]. Lattice points within the reciprocal lattice can be interconnected through the lattice vectors $(\mathbf{b}_1, \mathbf{b}_2, \mathbf{b}_3)$, which are derived from the lattice vectors $(\mathbf{a}_1, \mathbf{a}_2, \mathbf{a}_3)$ of the physical lattice according to the following relationship:

$$\mathbf{b}_1 = \frac{2\pi}{V}\mathbf{a}_2 \times \mathbf{a}_3 \tag{2}$$

and cyclic permutations, where $V = \mathbf{a}_1 \cdot (\mathbf{a}_2 \times \mathbf{a}_3)$ is the volume of the primitive unit cell in the physical space.

When considering that the physical lattice is bcc with the corresponding lattice vectors given in (1), the reciprocal lattice vectors are given by

$$\mathbf{b}_1 = \frac{4\pi}{a}\left(-\frac{1}{2}\hat{\mathbf{y}} - \frac{1}{2}\hat{\mathbf{z}}\right)$$

$$\mathbf{b}_2 = \frac{4\pi}{a}\left(\frac{1}{2}\hat{\mathbf{x}} + \frac{1}{2}\hat{\mathbf{y}}\right)$$

$$\mathbf{b}_3 = \frac{4\pi}{a}\left(\frac{1}{2}\hat{\mathbf{x}} + \frac{1}{2}\hat{\mathbf{z}}\right). \tag{3}$$

Fig. 2(a) illustrates the reciprocal lattice in this case, from which it can be found that this lattice is fcc. The points in the purple lattice in the upper left corner of the lattice arrangement are used to illustrate how the lattice points at the center of each face are connected to other lattice points using the reciprocal lattice vectors.

In reciprocal space, the WS cell, also known as the first Brillouin zone (BZ), displays the full symmetry of wavevectors and is widely used to analyze wave propagation properties, such as electromagnetic bandgaps and dispersion relations of periodic structures. When the unit cell in the direct space is highly symmetric, we can simplify the dispersion analysis by focusing on a subset of the BZ. The minimum region that contains all the information about wave propagation is called an irreducible BZ. The shape of the irreducible BZ is determined by the combined symmetry of the BZ and the actual unit cell. In Fig. 2(b), the BZ of the bcc structure is shown and takes the shape of a rhombic dodecahedron. Additionally, the possible irreducible BZ with the smallest volume is demonstrated by the black wireframe area. Taking into account (3), the coordinates of the vertices of the irreducible BZ can be obtained as follows:

$$\Gamma = (0, 0, 0)$$

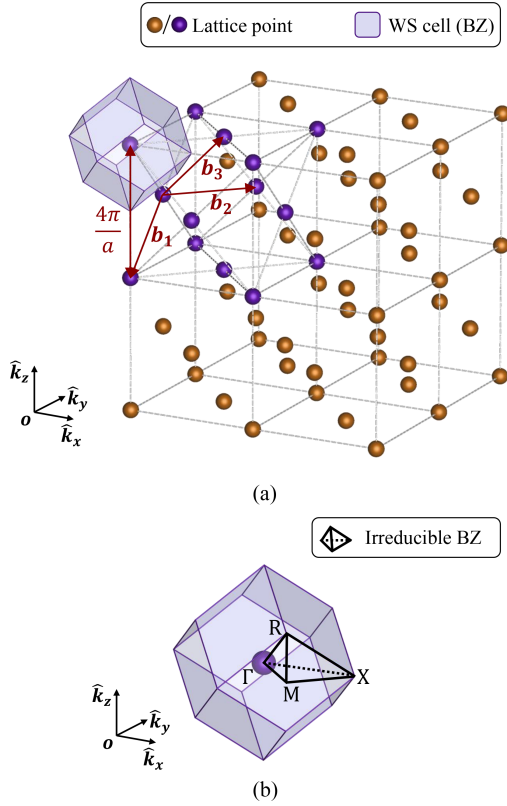$$X = \frac{4\pi}{a}\left(\frac{1}{2}, 0, 0\right)$$

(a)

(b)

FIGURE 2. (a) Reciprocal lattice when the 3D periodic structures are organized in the bcc configuration. The WS cell is highlighted in light purple. (b) Brillouin zone and irreducible Brillouin zone when the actual periodic unit cell is highly symmetric.

$$R = \frac{4\pi}{a}\left(\frac{1}{4}, -\frac{1}{4}, \frac{1}{4}\right)$$

$$M = \frac{4\pi}{a}\left(\frac{1}{4}, -\frac{1}{4}, 0\right). \tag{4}$$

Analysis of the dispersion properties of periodic structures is usually further simplified by studying the dispersion diagrams along the edges of the irreducible BZ, since these edges represent the boundaries of the dispersion properties. In the following analysis and examples, we will focus on demonstrating the one-dimensional (1D) dispersion diagrams of the periodic structure along the edge of the irreducible BZ, or 2D dispersion diagrams (also known as isofrequency maps) along the surface of the irreducible BZ. However, our proposed method is not limited to these dispersion diagrams. It can be used to obtain dispersion diagrams along any direction of interest in the reciprocal space, as well as the complete four-dimensional dispersion diagrams (phase shifts along every spatial direction versus frequency).

In this work, the dispersion diagrams are computed by making use of the eigenmode solver in ANSYS HFSS. In the remainder of this section, we will study a bcc structure in which the element of the actual unit cell is a metallic sphere, as shown in Fig. 3 (the host medium is assumed to be vaccum).
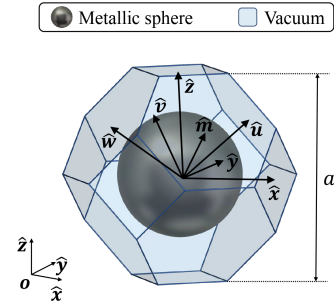

FIGURE 3. Wigner-Seigtz unit cell of a bcc structure in the direct space. Each unit cell contains a metallic sphere surrounded by vacuum.

The shape of the WS cell corresponding to this structure is a truncated octahedron of size a. The reciprocal lattice vectors of this bcc structure are given in (3), and the corresponding BZ and irreducible BZ areas are shown in Fig. 2(b). Taking this as an example, we will provide a detailed explanation of how to obtain the dispersion diagram along the specific contour $\overline{\Gamma R}$ of the irreducible BZ.

When using the HFSS eigenmode solver to obtain the dispersion diagram, it is necessary to define each pair of opposite faces on the WS cell as coupled ("Primary-Secondary") boundary conditions. For each pair of faces, we can define a unit vector normal to the faces. As illustrated in Fig. 3, the truncated octahedral-shaped WS cell involves seven pairs of coupled boundaries, with the corresponding unit vectors given by

$$\hat{\mathbf{x}} = (1, 0, 0)$$

$$\hat{\mathbf{y}} = (0, 1, 0)$$

$$\hat{\mathbf{z}} = (0, 0, 1)$$

$$\hat{\mathbf{u}} = \left(\frac{1}{\sqrt{3}}, \frac{1}{\sqrt{3}}, \frac{1}{\sqrt{3}}\right)$$

$$\hat{\mathbf{v}} = \left(-\frac{1}{\sqrt{3}}, \frac{1}{\sqrt{3}}, \frac{1}{\sqrt{3}}\right)$$

$$\hat{\mathbf{w}} = \left(-\frac{1}{\sqrt{3}}, -\frac{1}{\sqrt{3}}, \frac{1}{\sqrt{3}}\right)$$

$$\hat{\mathbf{m}} = \left(\frac{1}{\sqrt{3}}, -\frac{1}{\sqrt{3}}, \frac{1}{\sqrt{3}}\right). \tag{5}$$

To obtain the dispersion diagram along a given path in the BZ, it is necessary to accurately set the phase shift conditions in the simulator along the seven unit vectors defined in (5). For the path $\overline{\Gamma R}$, it is apparent from (4) that its corresponding wavevector is
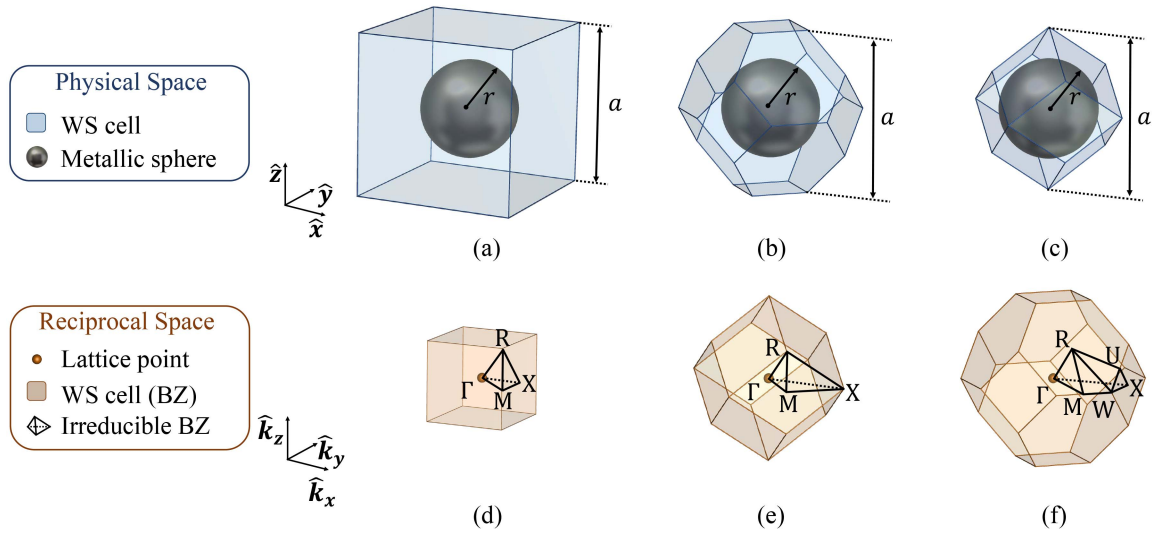
$$\mathbf{k}_{\Gamma R} = \frac{4\pi}{a}\left(\frac{1}{4}\hat{\mathbf{x}} - \frac{1}{4}\hat{\mathbf{y}} + \frac{1}{4}\hat{\mathbf{z}}\right) \tag{6}$$

with a phase associated with this wavevector along an arbitrary direction $\mathbf{r}$ in the physical space given by

$$\phi_{\mathbf{r}}(r) = \mathbf{k}_{\Gamma R} \cdot r\hat{\mathbf{r}}. \tag{7}$$

TABLE 1. Phase Shift Conditions Related to the Propagation Along the Edges of the Irreducible BZ for a Bcc Structure

	$\Delta\phi_x$	$\Delta\phi_y$	$\Delta\phi_z$	$\Delta\phi_u$	$\Delta\phi_v$	$\Delta\phi_w$	$\Delta\phi_m$
$\Gamma \to X$	$[0, 2\pi]$	$[0, 0]$	$[0, 0]$	$[0, \pi]$	$[0, -\pi]$	$[0, -\pi]$	$[0, \pi]$
$X \to M$	$[2\pi, \pi]$	$[0, -\pi]$	$[0, 0]$	$[\pi, 0]$	$[-\pi, -\pi]$	$[-\pi, 0]$	$[\pi, \pi]$
$M \to \Gamma$	$[\pi, 0]$	$[-\pi, 0]$	$[0, 0]$	$[0, 0]$	$[-\pi, 0]$	$[0, 0]$	$[\pi, 0]$
$\Gamma \to R$	$[0, \pi]$	$[0, -\pi]$	$[0, \pi]$	$[0, \pi/2]$	$[0, -\pi/2]$	$[0, \pi/2]$	$[0, 3\pi/2]$
$R \to X$	$[\pi, 2\pi]$	$[-\pi, 0]$	$[\pi, 0]$	$[\pi/2, \pi]$	$[-\pi/2, -\pi]$	$[\pi/2, -\pi]$	$[3\pi/2, \pi]$
$R \to M$	$[\pi, \pi]$	$[-\pi, -\pi]$	$[\pi, 0]$	$[\pi/2, 0]$	$[-\pi/2, -\pi]$	$[\pi/2, 0]$	$[3\pi/2, \pi]$

FIGURE 4. The WS cell for (a) sc, (b) bcc and (c) fcc configuration when the actual unit cell is composed of metallic spheres. BZ and irreducible BZ for (d) sc, (e) bcc and (f) fcc.

Along the x-direction (that is, $\mathbf{r} = x\hat{\mathbf{x}}$), the corresponding phase can be calculated as

$$\phi_{\mathbf{x}}(x) = \mathbf{k}_{\Gamma R} \cdot x\hat{\mathbf{x}} = \frac{4\pi}{a}\left(\frac{1}{4}\hat{\mathbf{x}} - \frac{1}{4}\hat{\mathbf{y}} + \frac{1}{4}\hat{\mathbf{z}}\right) \cdot x\hat{\mathbf{x}} = \pi\frac{x}{a}. \quad (8)$$

As the period along the x-direction for the unit cell under study is a, the phase along this direction varies from $\phi_{\mathbf{x}}(0) = 0$ to $\phi_{\mathbf{x}}(a) = \pi$. This means that the phase-shift range is

$$\Delta\phi_{\mathbf{x}} \in [0, \pi]. \quad (9)$$

Following a similar procedure, the phase-shift variation associated with the wavevector $\mathbf{k}_{\Gamma R}$ can be determined along the directions of other unit vectors. Once all phase shift ranges have been set up, the simulator directly gives us the dispersion diagram along the path $\overline{\Gamma R}$. Dispersion diagrams along other paths in the BZ, as well as the dispersion properties of other periodic structures, can be derived by analogies. Table 1 summarizes the phase shift conditions related to the propagation along the edges of the irreducible BZ for the bcc structure depicted in Fig. 3. In the Appendix, detailed information is

provided on the phase shift conditions associated with propagation along the edges of the irreducible BZ when the 3D periodic structures are organized in the fcc configuration.

III. SC, BCC, AND FCC STRUCTURES

In this section, the dispersion diagrams of periodic structures composed of metallic spheres and cuboids, arranged in sc, bcc, and fcc lattices, are analyzed and compared. The eigenmode solver of ANSYS HFSS is used to obtain the diagrams.

A. ARRANGEMENTS OF METALLIC SPHERES

When the spheres are arranged in the configurations of sc, bcc, and fcc, the WS cells associated with them are displayed in Fig. 4(a)–(c). The length of the cell along the Cartesian coordinate axis is the same for all of them, which is denoted as $a = 2\,\text{mm}$, and the diameter of the metallic spheres is also the same, being $2r = 0.6a = 1.2\,\text{mm}$. The host medium is assumed to be a vacuum.

Taking into account the spatial structure of the unit cell in three dimensions, it is found that for the sc configuration, the coordination number of the WS cell is 6, 8 for the bcc
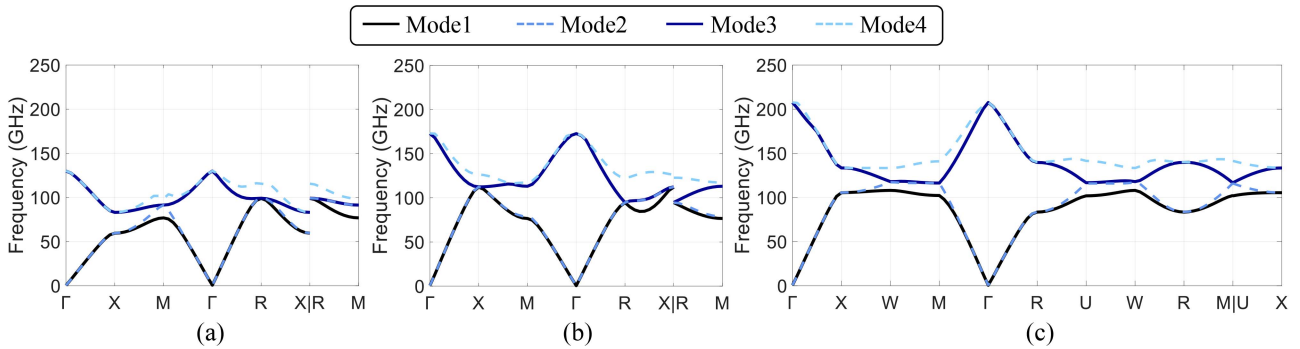
FIGURE 5. Dispersion diagrams of the first four modes in periodic arrangements of metallic spheres with lattices (a) sc, (b) bcc and (c) fcc.
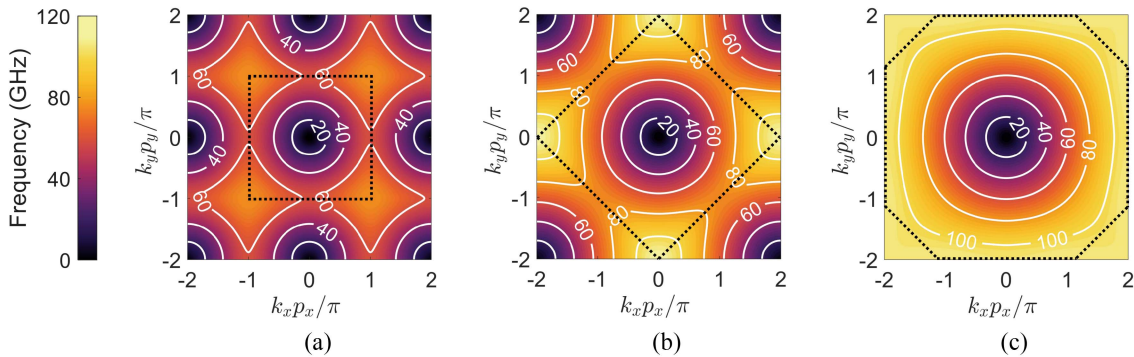

FIGURE 6. Isofrequency maps (2D dispersion diagram) of the fundamental mode in periodic arrangements of metallic spheres with lattices (a) sc, (b) bcc and (c) fcc. The area within the black dashed line is the first BZ.

configuration, and 12 for the fcc configuration. Consequently, the volume of the WS cells corresponding to the sc, bcc, and fcc configurations progressively decreases, indicating a gradual compaction of the periodic arrangement of metallic spheres.

Using the analysis introduced in Section II-B, the BZ and the irreducible BZ corresponding to these three periodic structures can be obtained, as shown in Fig. 4(d)–(f). As well reported elsewhere [14], when the physical lattice is sc, the reciprocal lattice retains the sc configuration. In contrast, when the physical lattice is bcc, the reciprocal lattice is fcc, and when the physical lattice is fcc, the reciprocal lattice adopts the bcc configuration. When comparing the BZ of these three cases, it is clear that the BZ of the periodic structure with the fcc configuration has the highest symmetry and is most similar to a spherical shape. This suggests that the dispersion properties of metallic spheres with a fcc arrangement are more isotropic.

Using the simulation setup described in Section II-B, the three periodic structures depicted in Fig. 4(a)–(c) were simulated to obtain their dispersion diagrams. The 1D dispersion diagrams along the edges of the irreducible BZ are shown in Fig. 5, and the isofrequency maps (2D dispersion diagram) in the plane $k_x k_y$ are shown in Fig. 6. As expected, the simulation results demonstrate that the dispersion gradually weakens

and the isotropy of the dispersion properties improves as the periodic structure configuration changes from sc to bcc to fcc.

B. ARRANGEMENTS OF METALLIC CUBOIDS

In this section, metallic cuboids are used as the elements of the unit cells and they are arranged in sc, bcc and fcc configurations. The host medium continues to be vacuum, as in previous sections. Fig. 7(a)–(c) show the unit cell of the three periodic structures under study. The length along the Cartesian coordinate axis is the same for the three cases; that is, $a = 2\,\text{mm}$. The dimensions of the cuboids in the three structures are also the same, with $l_x = 0.55a = 1.1\,\text{mm}$, $l_y = 0.35a = 0.7\,\text{mm}$, and $l_z = 0.15a = 0.3\,\text{mm}$.

Since the cuboid is no longer symmetric along the Cartesian axis, the shape of the corresponding irreducible BZs is no longer determined only by the symmetry of the BZ but is determined by the combined symmetry of the BZ and the actual unit cell. The irreducible BZs for sc, bcc, and fcc composed of metallic cuboids are shown in Fig. 7(d)–(f), respectively. It can be observed that, in comparison to the structures composed of metallic spheres, the volumes of the irreducible BZs relative to the BZ are now larger, caused by the lower level of symmetry of the periodic structure itself.

The effectiveness of the dispersion analysis method in Section II is not affected by the differences mentioned above.
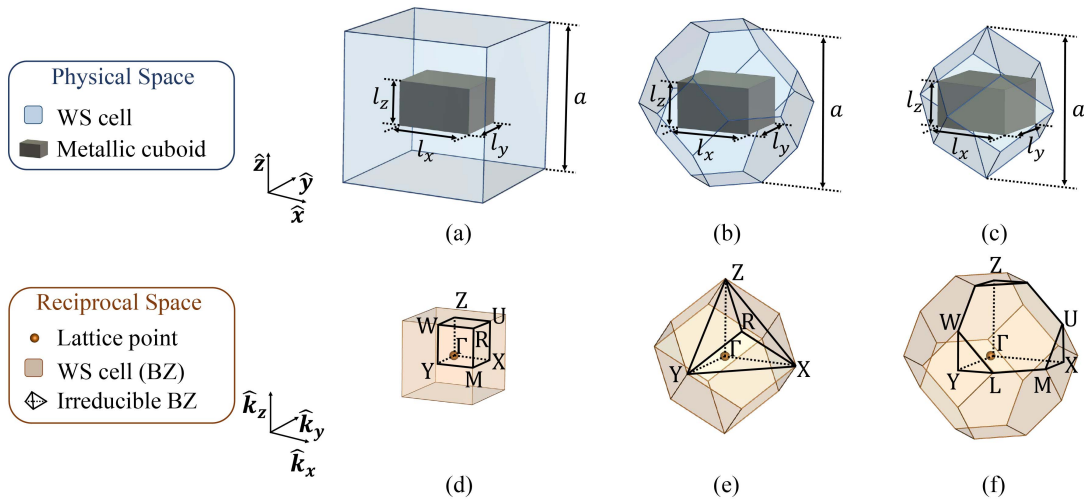
FIGURE 7. The WS cell for (a) sc, (b) bcc and (c) fcc configuration when the actual unit cell is composed of metallic cuboids. BZ and irreducible BZ for (d) sc, (e) bcc and (f) fcc.

To generate the dispersion diagram of the periodic structure made up of metallic cuboids, the same method and simulation setting as described in the analysis of metallic spheres in Section III-A can be used. Fig. 8 shows the isofrequency maps in the planes $k_x k_y$, $k_x k_z$, and $k_y k_z$ when the metallic cuboids have sc, bcc, and fcc configurations, respectively. It can be observed from the results that, due to variations in the actual unit cells across these three planes, the isofrequency maps in these planes also differ. This observation further confirms that the wave propagation is influenced by both the inherent symmetry of the BZ and the symmetry of the elements of the physical unit cell. Nevertheless, bcc and fcc structures usually have a lower level of dispersion over a wider range of frequencies than sc structures.

IV. MONOCLINIC STRUCTURE
In this section, we use the periodic monoclinic structure as an example to show the application of the analysis methods discussed in Section II for studying the dispersion properties of more complex noncubic structures. We start by analyzing the physical and reciprocal spaces of this structure. Then, we use metallic monoclinic elements as the unit cell to obtain dispersion diagrams through simulations in ANSYS HFSS.

A. PHYSICAL AND RECIPROCAL LATTICES
Fig. 9(a) illustrates the physical lattice of the periodic monoclinic stucture. The three side lengths of its corresponding WS cell are represented by a, b, and c (in the following analysis and calculation, it is assumed that a and b are smaller than c), and the angle smaller than $90°$ is represented by α. Based on this, the lattice vectors in physical space can be expressed as

$$\mathbf{a}_1 = a\hat{\mathbf{x}}$$

$$\mathbf{a}_2 = b\hat{\mathbf{y}}$$

$$\mathbf{a}_3 = c\left(\cos\alpha\,\hat{\mathbf{y}} + \sin\alpha\,\hat{\mathbf{z}}\right). \tag{10}$$

According to (2), the lattice vectors in the reciprocal space are then given by

$$\mathbf{b}_1 = \frac{2\pi}{a}\hat{\mathbf{x}}$$

$$\mathbf{b}_2 = \frac{2\pi}{b}\left(\hat{\mathbf{y}} - \cot\alpha\,\hat{\mathbf{z}}\right)$$

$$\mathbf{b}_3 = \frac{2\pi}{c\sin\alpha}\,\hat{\mathbf{z}} \tag{11}$$

with the corresponding reciprocal lattice and BZ shown in Fig. 9(b). It can be observed that the BZ of the monoclinic structure is a hexagonal prism. Although the hexagon corresponding to the hexagonal prism is not a regular hexagon, its opposite sides are equal and parallel to each other, and the entire hexagon is centrally symmetric.

If now the host medium is assumed to be vacuum and the element of the periodic structure is a piece of metal with a monoclinic shape, as shown in Fig. 10(a), three pairs of coupling boundaries are needed in HFSS to simulate the dispersion diagrams for this unit cell. The unit vectors perpendicular to these three pairs of boundaries are

$$\hat{\mathbf{x}} = (1, 0, 0)$$

$$\hat{\mathbf{z}} = (0, 0, 1)$$

$$\hat{\mathbf{u}} = (0, -\sin\alpha, \cos\alpha). \tag{12}$$

Taking into account the symmetry of the physical unit cell and the BZ, its irreducible BZ is one quarter of the BZ [as shown in Fig. 10(b)]. Based on the lattice vectors in the reciprocal space given in (11), the vertex coordinates of the irreducible BZ can be obtained as

$$\Gamma = (0, 0, 0)$$

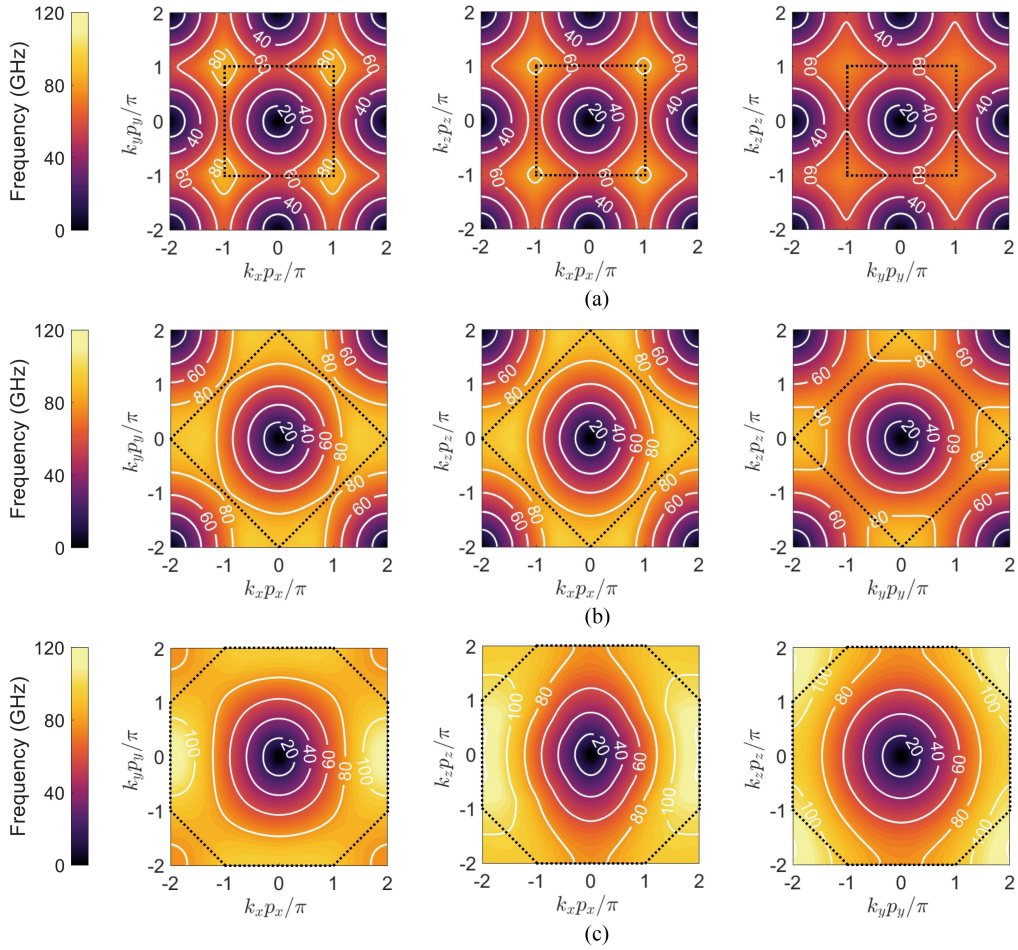$$Z = \left(0, 0, \frac{\pi}{c\sin\alpha}\right)$$

FIGURE 8. Isofrequency maps (2D dispersion diagram) of the fundamental mode in periodic arrangements of metallic cuboids with lattices (a) sc, (b) bcc and (c) fcc. The region within the black dashed line is the first BZ.

$$Z_1 = \left(0, 0, -\frac{\pi}{c \sin \alpha}\right)$$

$$U = \left(\frac{\pi}{a}, 0, \frac{\pi}{c \sin \alpha}\right)$$

$$U_1 = \left(\frac{\pi}{a}, 0, -\frac{\pi}{c \sin \alpha}\right)$$

$$M = \left(\frac{\pi}{a}, \left(\frac{\pi}{b} - \frac{\pi \cos \alpha}{c}\right)\frac{1}{\sin^2 \alpha}, \frac{\pi}{c \sin \alpha}\right)$$

$$M_1 = \left(\frac{\pi}{a}, \frac{2\pi}{b} - \left(\frac{\pi}{b} - \frac{\pi \cos \alpha}{c}\right)\frac{1}{\sin^2 \alpha}, \frac{\pi}{c \sin \alpha} - \frac{2\pi}{b} \cot \alpha\right)$$

$$M_2 = \left(\frac{\pi}{a}, \left(\frac{\pi}{b} - \frac{\pi \cos \alpha}{c}\right)\frac{1}{\sin^2 \alpha}, -\frac{\pi}{c \sin \alpha}\right)$$

$$W = \left(0, \left(\frac{\pi}{b} - \frac{\pi \cos \alpha}{c}\right)\frac{1}{\sin^2 \alpha}, \frac{\pi}{c \sin \alpha}\right)$$

$$W_1 = \left(0, \frac{2\pi}{b} - \left(\frac{\pi}{b} - \frac{\pi \cos \alpha}{c}\right)\frac{1}{\sin^2 \alpha}, \frac{\pi}{c \sin \alpha} - \frac{2\pi}{b} \cot \alpha\right)$$

$$W_2 = \left(0, \left(\frac{\pi}{b} - \frac{\pi \cos \alpha}{c}\right)\frac{1}{\sin^2 \alpha}, -\frac{\pi}{c \sin \alpha}\right). \quad (13)$$

As described in Section II-B, it is necessary to accurately set the phase-shift conditions along the $\hat{\mathbf{x}}$, $\hat{\mathbf{z}}$, and $\hat{\mathbf{u}}$ directions in the simulator to obtain the dispersion diagram along the path given in the reciprocal space. In essence, the approach and computational procedures outlined in Section II-B for the periodic arrangement with the bcc configuration are replicated. To provide a clearer explanation of the method, we will illustrate the detailed calculation process by focusing on the dispersion diagram along the $\overline{\Gamma M_1}$ path.

From (13) we find that the corresponding wavevector for the path $\overline{\Gamma M_1}$ is

$$\mathbf{k}_{\Gamma M_1} = \frac{\pi}{a}\hat{\mathbf{x}} + \left[\frac{2\pi}{b} - \left(\frac{\pi}{b} - \frac{\pi \cos \alpha}{c}\right)\frac{1}{\sin^2 \alpha}\right]\hat{\mathbf{y}}$$
$$+ \left(\frac{\pi}{c \sin \alpha} - \frac{2\pi}{b} \cot \alpha\right)\hat{\mathbf{z}}. \quad (14)$$

Along the x-direction, the phase associated with this wavevector can be calculated as

$$\phi_{\mathbf{x}}(x) = \mathbf{k}_{\Gamma M_1} \cdot x\hat{\mathbf{x}} = \frac{\pi}{a}x. \quad (15)$$
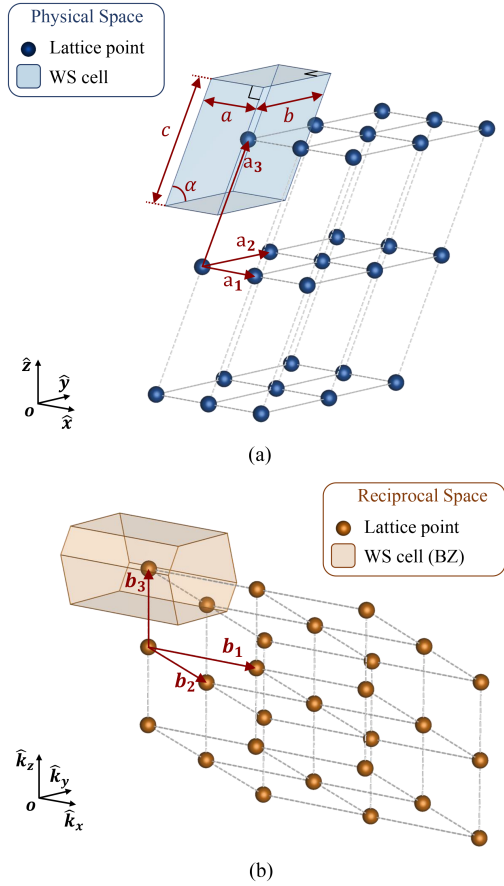
FIGURE 9. (a) Physical lattice and (b) reciprocal lattice for the monoclinic structure.
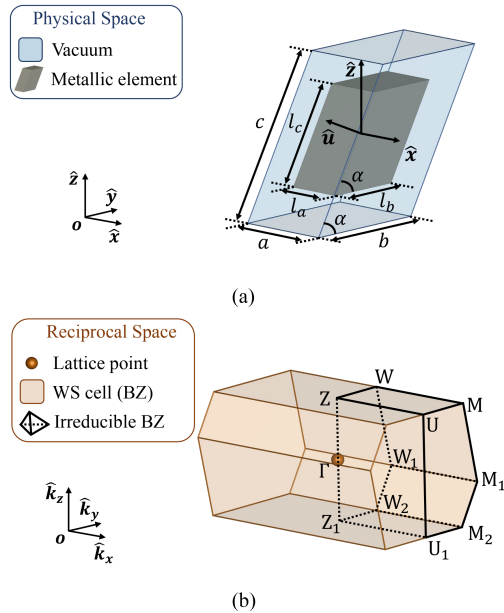

FIGURE 10. (a) The WS cell for monoclinic configuration when the actual unit cell is composed of metallic element with a monoclinic shape. (b) BZ and irreducible BZ for the periodic structure in pannel (a).

TABLE 2. Phase Shift Conditions Related to Propagation From the Origin Γ to the Vertices of the Irreducible BZ for Monoclinic Periodic Structures

	$\Delta\phi_x$	$\Delta\phi_z$	$\Delta\phi_u$
$\Gamma \to Z$	$[0,0]$	$[0,\pi]$	$[0, \frac{b\cos\alpha\pi}{c}]$
$\Gamma \to Z_1$	$[0,0]$	$[0,-\pi]$	$[0, -\frac{b\cos\alpha\pi}{c}]$
$\Gamma \to U$	$[0,\pi]$	$[0,\pi]$	$[0, \frac{b\cos\alpha\pi}{c}]$
$\Gamma \to U_1$	$[0,\pi]$	$[0,-\pi]$	$[0, -\frac{b\cos\alpha\pi}{c}]$
$\Gamma \to M$	$[0,\pi]$	$[0,\pi]$	$[0, \frac{2b\cos\alpha\pi}{c} - \pi]$
$\Gamma \to M_1$	$[0,\pi]$	$[0, -\frac{2c\cos\alpha\pi}{b} + \pi]$	$[0,-\pi]$
$\Gamma \to M_2$	$[0,\pi]$	$[0,-\pi]$	$[0,-\pi]$
$\Gamma \to W$	$[0,0]$	$[0,\pi]$	$[0, \frac{2b\cos\alpha\pi}{c} - \pi]$
$\Gamma \to W_1$	$[0,0]$	$[0, -\frac{2c\cos\alpha\pi}{b} + \pi]$	$[0,-\pi]$
$\Gamma \to W_2$	$[0,0]$	$[0,-\pi]$	$[0,-\pi]$

As the period along the x-direction for the unit cell under study is a, the phase along this direction varies from $\phi_\mathbf{x}(0) = 0$ to $\phi_\mathbf{x}(a) = \pi$. This means that the phase-shift range is

$$\Delta\phi_\mathbf{x} \in [0, \pi] . \qquad (16)$$

Similarly, along the z-direction, the phase associated with this wavevector is

$$\phi_\mathbf{z}(z) = \mathbf{k}_{\Gamma M_1} \cdot z\hat{\mathbf{z}} = \left(\frac{\pi}{c\sin\alpha} - \frac{2\pi}{b}\cot\alpha \right) z . \qquad (17)$$

Along the z-direction, the period of the unit cell is $c\sin\alpha$, which makes the phase along this direction vary from $\phi_\mathbf{z}(0) = 0$ to $\phi_\mathbf{z}(c\sin\alpha) = -2(c/b)\cos\alpha\pi + \pi$. The phase-shift range is then given by

$$\Delta\phi_\mathbf{z} \in \left[0, -\frac{2c\cos\alpha\pi}{b} + \pi \right] . \qquad (18)$$

Along the u-direction, we find

$$\phi_\mathbf{u}(u) = \mathbf{k}_{\Gamma M_1} \cdot u\hat{\mathbf{u}} = -\frac{\pi}{b\sin\alpha} u . \qquad (19)$$

Since the period along the u-direction for the unit cell under study is $b\sin\alpha$, the phase along this direction varies from $\phi_\mathbf{u}(0) = 0$ to $\phi_\mathbf{u}(b\sin\alpha) = -\pi$. The phase-shift range for this direction is

$$\Delta\phi_\mathbf{u} \in [0, -\pi] . \qquad (20)$$

For the simulation of the dispersion diagrams along the other paths, the corresponding phase shift conditions can be calculated following the same steps. In Table 2, for simplicity, we only summarize the phase shift conditions corresponding to the propagation from the origin Γ to the vertices of the irreducible BZ. The phase shift related to propagation along the irreducible edge of the BZ can be derived from Table 2 through simple deformation.
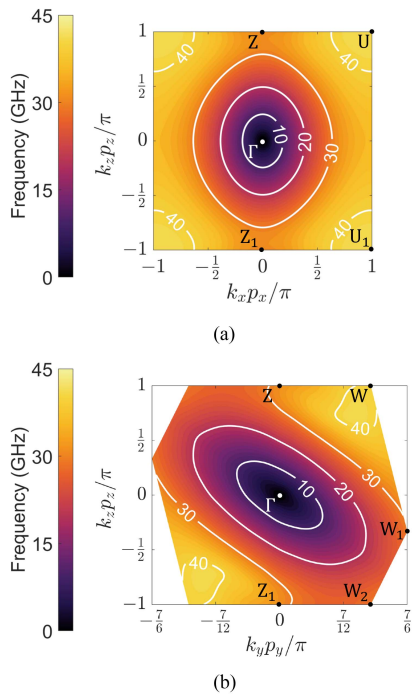
FIGURE 11. Isofrequency maps (2D dispersion diagram) of the fundamental mode on the (a) $k_x k_z$ plane and (b) $k_y k_z$ plane when the actual unit cell is metallic monoclicnic element and the periodic structure arranged by monoclicnic configuration. Only the results within the first BZ are shown.

B. DISPERSION ANALYSIS

As illustrated in Fig. 10(a), a monoclinic-shaped metallic piece is taken as the element of the actual unit cell, and the host medium is considered to be a vacuum. We assume that the side lengths of the monoclinic unit cell are $a = 2$ mm, $b = 3$ mm, and $c = 4$ mm, with $\alpha = \pi/3$. The metallic element has dimensions $l_a = 0.6a = 1.2$ mm, $l_b = 0.6b = 1.8$ mm, and $l_c = 0.6c = 2.4$ mm. By substituting these values into (13), we can calculate the vertices of the irreducible BZ for this periodic structure. Following the guidelines of Section IV-A, we can generate the corresponding dispersion diagrams in HFSS. Thus, in Fig. 11(a) and (b) we show the isofrequency maps obtained for the fundamental mode of this monoclinic structure in the planes $k_x k_z$ and $k_y k_z$. It can be observed that the isofrequency map in the $k_y k_z$ plane is centrosymmetric, while the isofrequency map in the $k_x k_z$ plane is symmetric about the k_x and k_z axes. This observation aligns with the symmetry characteristics of the BZ for this monoclinic structure.

V. CONCLUSION

The methodology presented in this article outlines the process for conducting dispersion analysis of 3D periodic structures using the eigenmode solver of commercial electromagnetic simulation software. First, we review some basic concepts in both physical and reciprocal spaces, describing the relationship between lattices in these domains. Taking the bcc structure as an example, we provide detailed steps to perform
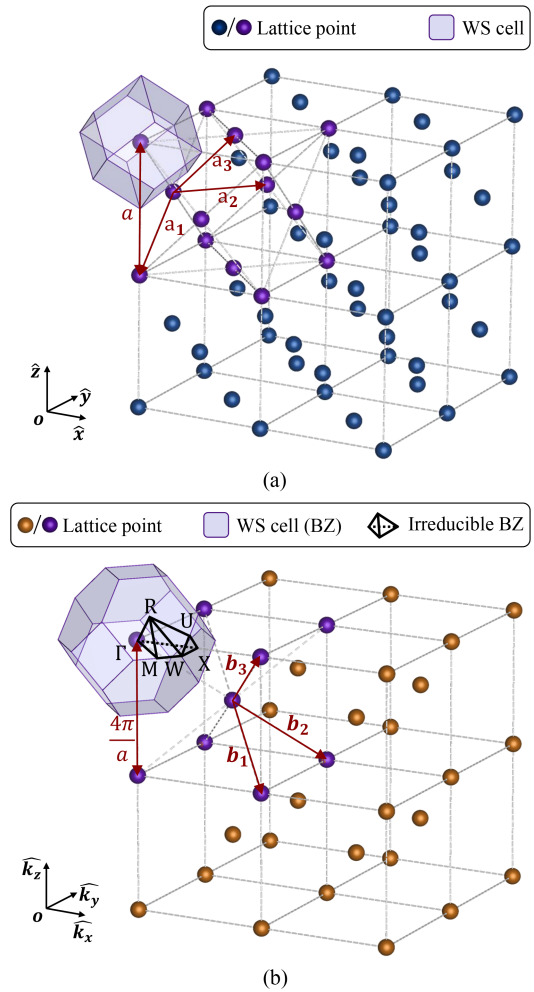

FIGURE 12. (a) Physical lattice and (b) reciprocal lattice for the fcc structure.

the dispersion analysis in ANSYS HFSS and explain how to set the appropriate conditions in the simulator. We studied the dispersion characteristics of metallic spheres and cuboids when they were arranged in sc, bcc, and fcc configurations. The results show that the bcc and fcc configurations have advantageous properties, including enhanced isotropy in a broader frequency range. Using the analysis of the monoclinic configuration as an example, it is demonstrated that the methods described in this study can be easily extended to other 3D periodic structures with noncubic lattices. The aim is to provide more design versatility and increase the potential of microwave and antenna devices based on 3D periodic structures.

APPENDIX

In this Appendix, we provide a detailed analysis of the physical and reciprocal lattices of fcc periodic structure, as well as how to set the conditions in the HFSS eigenmode solver to obtain the dispersion diagrams of it.

Fig. 12(a) illustrates an fcc lattice, as well as the connectivity relationships between a given lattice point and its

TABLE 3. Phase Shift Conditions Related to Propagation Along the Edges of the Irreducible BZ for Fcc Periodic Structures

	$\Delta\phi_u$	$\Delta\phi_v$	$\Delta\phi_w$	$\Delta\phi_m$	$\Delta\phi_p$	$\Delta\phi_q$
$\Gamma \to X$	$[0,\pi]$	$[0,0]$	$[0,-\pi]$	$[0,0]$	$[0,\pi]$	$[0,\pi]$
$X \to W$	$[\pi,\pi]$	$[0,-\pi/2]$	$[-\pi,-\pi]$	$[0,\pi/2]$	$[\pi,3\pi/2]$	$[\pi,\pi/2]$
$W \to M$	$[\pi,3\pi/4]$	$[-\pi/2,-3\pi/4]$	$[-\pi,-3\pi/4]$	$[\pi/2,3\pi/4]$	$[3\pi/2,3\pi/2]$	$[\pi/2,0]$
$M \to \Gamma$	$[3\pi/4,0]$	$[-3\pi/4,0]$	$[-3\pi/4,0]$	$[3\pi/4,0]$	$[3\pi/2,0]$	$[0,0]$
$\Gamma \to R$	$[0,\pi]$	$[0,0]$	$[0,0]$	$[0,\pi]$	$[0,\pi]$	$[0,0]$
$R \to U$	$[\pi,5\pi/4]$	$[0,0]$	$[0,-3\pi/4]$	$[\pi,\pi/2]$	$[\pi,5\pi/4]$	$[0,3\pi/4]$
$U \to W$	$[5\pi/4,\pi]$	$[0,-\pi/2]$	$[-3\pi/4,-\pi]$	$[\pi/2,\pi/2]$	$[5\pi/4,3\pi/2]$	$[3\pi/4,\pi/2]$
$W \to R$	$[\pi,\pi]$	$[-\pi/2,0]$	$[-\pi,0]$	$[\pi/2,\pi]$	$[3\pi/2,\pi]$	$[\pi/2,0]$
$R \to M$	$[\pi,3\pi/4]$	$[0,-3\pi/4]$	$[0,-3\pi/4]$	$[\pi,3\pi/4]$	$[\pi,3\pi/2]$	$[0,0]$
$U \to X$	$[5\pi/4,\pi]$	$[0,0]$	$[-3\pi/4,-\pi]$	$[\pi/2,0]$	$[5\pi/4,\pi]$	$[3\pi/4,\pi]$

neighbors for the purple points in the upper left corner. Assuming the side length of the cube in this upper left corner is a, the direct-space lattice vectors are given by

$$\mathbf{a}_1 = a\left(-\frac{1}{2}\hat{\mathbf{y}} - \frac{1}{2}\hat{\mathbf{z}}\right)$$

$$\mathbf{a}_2 = a\left(\frac{1}{2}\hat{\mathbf{x}} + \frac{1}{2}\hat{\mathbf{y}}\right)$$

$$\mathbf{a}_3 = a\left(\frac{1}{2}\hat{\mathbf{x}} + \frac{1}{2}\hat{\mathbf{z}}\right) \tag{21}$$

and, according to (2), the corresponding lattice vectors [see Fig. 12(b)] in the reciprocal space are

$$\mathbf{b}_1 = \frac{4\pi}{a}\left(\frac{1}{2}\hat{\mathbf{x}} - \frac{1}{2}\hat{\mathbf{y}} - \frac{1}{2}\hat{\mathbf{z}}\right)$$

$$\mathbf{b}_2 = \frac{4\pi}{a}\left(\frac{1}{2}\hat{\mathbf{x}} + \frac{1}{2}\hat{\mathbf{y}} - \frac{1}{2}\hat{\mathbf{z}}\right)$$

$$\mathbf{b}_3 = \frac{4\pi}{a}\left(\frac{1}{2}\hat{\mathbf{x}} - \frac{1}{2}\hat{\mathbf{y}} + \frac{1}{2}\hat{\mathbf{z}}\right) . \tag{22}$$

In Fig. 12(b), the BZ of the fcc structure is highlighted in light purple, and its irreducible BZ is represented by black lines. By using (22), the following coordinates of the vertices of the irreducible BZ are found:

$$\Gamma = (0,0,0)$$

$$X = \frac{4\pi}{a}\left(\frac{1}{2}, 0, 0\right)$$

$$W = \frac{4\pi}{a}\left(\frac{1}{2}, -\frac{1}{4}, 0\right)$$

$$M = \frac{4\pi}{a}\left(\frac{3}{8}, -\frac{3}{8}, 0\right)$$

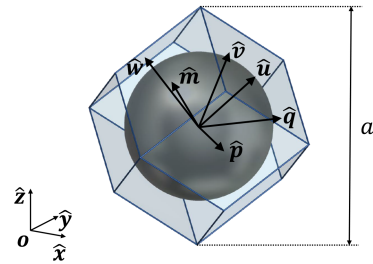$$R = \frac{4\pi}{a}\left(\frac{1}{4}, -\frac{1}{4}, \frac{1}{4}\right)$$

FIGURE 13. Periodic structure with fcc configuration, whose actual unit cell is created by a periodic repetition of a metallic sphere. *a* is the length of the corresponding WS cell along a Cartesian coordinate axis.

$$U = \frac{4\pi}{a}\left(\frac{1}{2}, -\frac{1}{8}, \frac{1}{8}\right) . \tag{23}$$

When a metallic sphere is taken as the element of the unit cell, with vacuum as the surrounding medium, the resulting unit cell is represented in Fig. 13, with a being the length of the WS cell along the Cartesian coordinate axis. In the HFSS eigenmode solver, the pair of opposite surfaces of the unit cell is defined as coupled ('Primary-Secondary') boundary conditions. For this rhombic dodecahedron shape, it results in six pairs of coupling boundaries, with the following directional unit vectors associated with these pairs:

$$\hat{\mathbf{u}} = \left(\frac{1}{\sqrt{2}}, 0, \frac{1}{\sqrt{2}}\right)$$

$$\hat{\mathbf{v}} = \left(0, \frac{1}{\sqrt{2}}, \frac{1}{\sqrt{2}}\right)$$

$$\hat{\mathbf{w}} = \left(-\frac{1}{\sqrt{2}}, 0, \frac{1}{\sqrt{2}}\right)$$

$$\hat{\mathbf{m}} = \left(0, -\frac{1}{\sqrt{2}}, \frac{1}{\sqrt{2}}\right)$$

$$\hat{\mathbf{p}} = \left(\frac{1}{\sqrt{2}}, -\frac{1}{\sqrt{2}}, 0 \right)$$

$$\hat{\mathbf{q}} = \left(\frac{1}{\sqrt{2}}, \frac{1}{\sqrt{2}}, 0 \right) . \tag{24}$$

Following the same calculation procedures as in Section II-B, the phase-shift conditions for the different sets of boundaries related to propagation along the edges of the irreducible BZ are summarized in Table 3.

REFERENCES

[1] W. Rotman and A. A. Oliner, "Periodic structures in trough waveguides," *Proc. IRE*, vol. 34, pp. 134–142, 1956.

[2] P. J. Crepeau and P. R. McIsaac, "Consequences of symmetry in periodic structures," *Proc. IEEE*, vol. 52, no. 1, pp. 33–43, Jan. 1964.

[3] A. Ishimaru, "Radiation from periodic structures excited by an aperiodic source," *IEEE Trans. Antennas Propag.*, vol. AP-13, no. 3, pp. 354–364, May 1965.

[4] A. Hessel, M. H. Chen, R. C. M. Li, and A. A. Oliner, "Propagation in periodically loaded waveguides with higher symmetries," *Proc. IEEE*, vol. 61, no. 2, pp. 183–195, Feb. 1973.

[5] C. Elachi, "Waves in active and passive periodic structures; a review," *Proc. IEEE*, vol. 64, no. 12, pp. 1666–1698, Dec. 1976.

[6] C. Larson and B. Munk, "The broad-band scattering response of periodic arrays," *IEEE Trans. Antennas Propag.*, vol. AP-31, no. 2, pp. 261–267, Mar. 1983.

[7] O. Quevedo-Teruel et al., "Roadmap on metasurfaces," *J. Opt.*, vol. 21, no. 7, 2019, Art. no. 073002.

[8] B. A. Mouris et al., "Glide symmetry applied to printed common-mode rejection filters," *IEEE Trans. Micorw. Theory Techn.*, vol. 70, no. 2, pp. 1198–1210, Feb. 2022.

[9] M. Bouslama, M. Traii, T. A. Denidni, and A. Gharsallah, "Beam-switching antenna with a new reconfigurable frequency selective surface," *IEEE Antennas Wireless Propag. Lett.*, vol. 15, pp. 1159–1162, 2016.

[10] M. Hussein, J. Zhou, Y. Huang, and B. Al-Juboori, "A low-profile miniaturized second-order bandpass frequency selective surface," *IEEE Antennas Wireless Propag. Lett.*, vol. 16, pp. 2791–2794, 2017.

[11] X. Zeng, Q. Chen, O. Zetterstrom, and O. Quevedo-Teruel, "Fully metallic glide-symmetric leaky-wave antenna at Ka-band with lens-augmented scanning," *IEEE Trans. Antennas Propag.*, vol. 70, no. 8, pp. 7158–7163, Aug. 2022.

[12] J. W. Yang, W. Y. Lai, H. C. Chou, and M. N. M. Kehn, "Compact Mikaelian lens synthesized by metasurfaces," *IEEE Antennas Wireless Propag. Lett.*, vol. 17, no. 3, pp. 397–400, Mar. 2018.

[13] C. Pfeiffer and A. Grbic, "A printed, broadband Luneburg lens antenna," *IEEE Trans. Antennas Propag.*, vol. 58, no. 9, pp. 3055–3059, Sep. 2010.

[14] N. W. Ashcroft and N. D. Mermin, *Solid State Physics*. Philadelphia, PA, USA: Saunders College, 1976.

[15] R. E. Collin, *Field Theory of Guided Waves*. Hoboken, NJ, USA: Wiley, 1990.

[16] J. D. Joannopoulos, S. G. Johnson, J. N. Winn, and R. D. Meade, *Photonic Crystals: Molding the Flow of Light*, 2nd ed. Princeton, NJ USA: Princeton Univ. Press, 2008.

[17] A. Alex-Amor, A. Palomares-Caballero, F. Mesa, O. Quevedo-Teruel, and P. Padilla, "Dispersion analysis of periodic structures in anisotropic media: Application to liquid crystals," *IEEE Trans. Antennas Propag.*, vol. 70, no. 4, pp. 2811–2821, Apr. 2022.

[18] E. Erfani, M. Niroo-Jazi, and S. Tatu, "A high-gain broadband gradient refractive index metasurface lens antenna," *IEEE Trans. Antennas Propag.*, vol. 64, no. 5, pp. 1968–1973, May 2016.

[19] K. Singh, M. U. Afzal, and K. P. Esselle, "Designing efficient phase-gradient metasurfaces for near-field meta-steering systems," *IEEE Access*, vol. 9, pp. 109080–109093, 2021.

[20] O. Bjorkqvist, O. Zetterstrom, and O. Quevedo-Teruel, "Additive manufactured dielectric Gutman lens," *Electron. Lett.*, vol. 55, no. 25, pp. 1318–1320, 2019.

[21] H. Wang, Q. Chen, O. Zetterstrom, and O. Quevedo-Teruel, "Three-dimensional broadband and isotropic double-mesh twin-wire media for meta-lenses," *Appl. Sci.*, vol. 11, no. 15, 2021, Art. no. 7153.

[22] I. Vendik, M. Odit, and D. Kozlov, "3D metamaterial based on a regular array of resonant dielectric inclusions," *Radio Eng.*, vol. 18, no. 2, pp. 111–116, 2009.

[23] O. Zetterstrom, N. J. G. Fonseca, and O. Quevedo-Teruel, "Additively manufactured half-Gutman lens antenna for mobile satellite communications," *IEEE Antennas Wireless Propag. Lett.*, vol. 22, no. 4, pp. 759–763, Apr. 2023.

[24] H. Wang, O. Zetterstrom, P. Castillo-Tapia, F. Mesa, and O. Quevedo-Teruel, "Analysis of the dispersion diagrams of 3D cubic periodic arrangements of metallic spheres," in *Proc. 18th Eur. Conf. Antennas Propag.*, 2024.

[25] G. Valerio, Z. Sipus, A. Grbic, and O. Quevedo-Teruel, "Accurate equivalent-circuit descriptions of thin glide-symmetric corrugated metasurfaces," *IEEE Trans. Antennas Propag.*, vol. 65, no. 5, pp. 2695–2700, May 2017.

[26] F. Bongard, J. Perruisseau-Carrier, and J. R. Mosig, "Enhanced periodic structure analysis based on a multiconductor transmission line model and application to metamaterials," *IEEE Trans. Microw. Theory Techn.*, vol. 57, no. 11, pp. 2715–2726, Nov. 2009.

[27] F. Mesa, G. Valerio, R. Rodríguez-Berral, and O. Quevedo-Teruel, "Simulation-assisted efficient computation of the dispersion diagram of periodic structures," *IEEE Antennas Propag. Mag.*, vol. 63, no. 5, pp. 33–45, Oct. 2021.

[28] F. Giusti, Q. Chen, F. Mesa, M. Albani, and O. Quevedo-Teruel, "Efficient Bloch analysis of general periodic structures with a linearized multimodal transfer-matrix approach," *IEEE Trans. Antennas Propag.*, vol. 70, no. 7, pp. 5555–5562, Jul. 2022.

[29] G. Valerio, S. Paulotto, P. Baccarelli, P. Burghignoli, and A. Galli, "Accurate Bloch analysis of 1-D periodic lines through the simulation of truncated structures," *IEEE Trans. Antennas Propag.*, vol. 59, no. 6, pp. 2188–2195, Jun. 2011.

HAIRU WANG (Graduate Student Member, IEEE) received the bachelor's degrees in information engineering from the Southeast University, Nanjing, China, in 2021, and the master's degree in science from the KTH Royal Institute of Technology, Stockholm, Sweden, in 2022. Since 2022, she has been working toward the Ph.D. degree in antennas and electromagnetics with the Division of Electromagnetic Engineering and Fusion Science (EMF), KTH. Her research interests include periodic structures and beamforming network.

OSKAR ZETTERSTROM (Graduate Student Member, IEEE) received the B.Sc., M.Sc., and Lic. degrees in electrical and electromagnetic engineering from the KTH Royal Institute of Technology, Stockholm, Sweden, in 2016, 2019, and 2021, respectively. Since 2019, he has been working toward the Ph.D. degree in antennas and electromagnetics with the Division of Electromagnetic Engineering, KTH. He has authored or coauthored more than 70 peer-reviewed journal and conference papers. His research interests include transformation optics, lens antennas, periodic structures possessing higher symmetries, and leaky-wave antennas. He was the recipient of the first price in the student design competition at APS/URSI 2016, Best Student Paper Award at URSI Spain 2020, and Best Antenna Technology Paper Award at EuCAP 2022 for his works. He is also a member of the EurAAP working group for Early Careers in Antennas and Propagation (ECAP), where he is responsible for the ECAP mentoring program.

PILAR CASTILLO-TAPIA (Graduate Student Member, IEEE) received the bachelor's and master's degrees in telecommunications engineering from the University of Zaragoza, Zaragoza, Spain, in 2017 and 2019, respectively. She is currently working toward the Ph.D. degree in highly-efficient integrated millimeter band antennas with the KTH Royal Institute of Technology, Stockholm, Sweden. Her research interests include lens antennas, metasurfaces possessing higher symmetries, and computational electromagnetics. She was the recipient of the first place in student paper competition at the 2022 International Symposium on Antennas and Propagation. She is also responsible for the EurAAP Early Careers and Women in Antennas and Propagation Mentoring Program.

FRANCISCO MESA (Fellow, IEEE) received the Licenciado and Ph.D. degrees in physics from the Universidad de Sevilla, Seville, Spain, in 1989 and 1991, respectively. He is currently a Professor with the Departamento de Física Aplicada 1, Universidad de Sevilla. His research interests include electromagnetic propagation/radiation in microwave and quasi-optical structures.

OSCAR QUEVEDO-TERUEL (Fellow, IEEE) received the Telecommunication Engineering and Ph.D. degrees from Carlos III University of Madrid, Spain, in 2005 and 2010, respectively. From 2010 to 2011, he was with the Department of Theoretical Physics of Condensed Matter, Universidad Autonoma de Madrid, Madrid, Spain, as a Research Fellow and went on to continue his postdoctoral research with the Queen Mary University of London, London, U.K., from 2011 to 2013. In 2014, he joined KTH Royal Institute of Technology, Stockholm, Sweden, where he is currently a Professor at the Division of Electrical Engineering and Fusion Science and the Director of the Master Programme in Electromagnetics, Fusion and Space Engineering. He is the co-author of more than 140 papers in international journals and 250 papers at international conferences. He was an Associate Editor for IEEE TRANSACTIONS ON ANTENNAS AND PROPAGATION from 2018 to 2022 and has been the Track Editor since 2022. He has also been the founder and Editor-in-Chief of the European Association on Antennas and Propagation (EurAAP) journal *Reviews of Electromagnetics* since 2020. Since 2021, he has been a member of the EurAAP Board of Directors. Since 2022, he has been the Vice-Chair of EurAAP. From 2019 to 2021, he was a distinguished Lecturer of the IEEE Antennas and Propagation Society. Since 2020, he has been the Chair of the IEEE APS Educational Initiatives Programme. He has made scientific contributions to higher symmetries, transformation optics, lens antennas, metasurfaces, and high-impedance surfaces.